On the Position Optimization of IRS

Jianyue Zhu, Yongming Huang, Jiaheng Wang, Keivan Navaie, Wei Huang, Zhiguo Ding

***Abstract*—The intelligent reflecting surface (IRS) technology is emerged as an enabling technology for beyond 5G systems and IoT networks in which the signal propagation is reconfigured to enhance wireless system performance. IRS consists of many passive elements and each reflecting the incident signal with a certain phase shift to collectively achieve the required beamforming. The IRS is to be a low profile and lightweight setting with a conformal geometry hence its position can be easily engineered to achieve certain performance enhancements. In the current literature, however, the flexibility in the IRS position is often overlooked since it is considered as a given fixture. We argue that optimizing the IRS position provides a new degree of freedom in the network design and enables extra performance gain. In this paper, we analytically characterize the optimal IRS's position to maximize the achievable system rate. We then obtain the optimal IRS positions for different IRS settings with fixed-height and variable-height and consider both cost-efficient equal phase shift IRS, and non-equal phase shift IRS that enables sophisticated beamforming. We further incorporate antenna directivity in our analysis and investigate its effect on the optimal IRS position in each case. Simulation results show that the provided optimal position yields higher performance than settings with random IRS locations. Our results provide significant practical insights on the network coverage design using the IRS.**

***Index Terms*—Intelligent reflecting surface, equal phase shift, non-equal phase shift, variable-height, fixed-height, system rate maximization**

I. Introduction

Motivated by the explosive demand of Internet of Thing (IoT), there are ever-increasing requirements of higher capacity in beyond fifth generation (5G) communication systems and IoT networks [1]–[3]. In order to meet this goal, various technologies, such as massive multiple-input multiple-output (MIMO) [4], millimeter wave (mmWave) [5], and small cells [6], have been proposed in recent years. However, the existing technologies generally require increased energy consumption and hardware cost due to the installing of costly radio frequency (RF) chains operating at higher frequency bands. Therefore, it is still an open problem to find innovative, spectral and energy efficient, and yet cost-effective solutions for beyond 5G systems and the IoT networks.

J. Zhu is with the College of Electronic and Information Engineering, Nanjing University of Information Science and Technology, Nanjing, China. (email: zhujy@nuist.edu.cn).

Y. Huang, J. Wang are with the National Mobile Communications Research Laboratory, Southeast University, Nanjing, China. (email: {zhujy, huangym, jhwang}@seu.edu.cn).

K. Navaie is with the School of Computing and Communications, Lancaster University, Lancaster, United Kingdom (email: k.navaie@lancaster.ac.uk).

W. Huang is with School of Computer Science and Information Engineering, Hefei University of Technology, Hefei, China. (email: huangwei@hfut.edu.cn)

Z. Ding is with the School of Electrical and Electronic Engineering, Manchester University, Manchester, United Kingdom (email: zhiguo.ding@manchester.ac.uk).

Recently, intelligent reflecting surface (IRS) has been proposed as a promising new technology for reconfiguring the propagation environment [7]–[9]. IRS is a planar surface consisting of a large number of low-cost passive reflecting elements. The reflecting elements are capable of inducing independent phase change to the incident signal independently and hence achieving three-dimensional (3D) reflecting beamforming. IRS has a lower hardware cost and energy consumption than that of the conventional active beamforming via multiple antennas. This is mainly because IRS needs no signal amplification and regeneration. Moreover, IRS is always low profile, lightweight, and has a conformal geometry, which enables its easy installation on the wall or ceiling [10]–[12].

Usually, IRS operates as a multi-antenna relay. The IRS-assisted wireless communication has been widely studied. For example, in [13], [14], the active transmit beamforming at the base station (BS) and the passive reflect beamforming at the IRS were jointly optimized in the IRS-assisted communication system. In addition, several works focus on the positioning problem with the assistance of an IRS. For example, in [15], the authors studied the fundamental limits of positioning with the aid of an IRS in mmWave systems. The authors in [16] proposed the Fisher-information matrix and Cramer-Rao lower bounds for positioning with IRS.

There are also other relevant topics on IRS, such as non-orthogonal multiple access (NOMA) [17]–[19], physical layer security [20]–[22], mmWave communications [23], [24], wireless power transfer (WPT) [25], [26], deep learning [27], [28], and unmanned aerial vehicle (UAV) communications [29], [30]. For example, in [17]–[19], the authors integrated NOMA and IRS and proposed using IRS to facilitate the implementation of NOMA. Also [20]–[22] leveraged the IRS for the implementation of physical layer security in wireless communication systems. IRSs were also proposed in [23], [24] to provide effective reflected paths and hence enhances coverage of mmWave signals. To improve WPT efficiency, IRS has been used in the IoT devices to create an efficient charging zone [25], [26]. Deep learning was adopted in [27], [28] for configuring the IRSs to improve the efficiency of wireless communications. The potential of the IRS in enhancing UAV communications was also demonstrated in [29], [30].

The key point of the employment of the IRS in the wireless communication system is its capability to reconfigure propagation environment [17], [31]. In the literature, the IRS is always assumed to be fixed in one position. Nevertheless, considering movable IRS significantly enhances its capability to reconfigure the propagation environment, we can design the IRS position to achieve the best performance.

In this work, we focus on the optimization of the IRS's position. Given the production costs, the IRS with equal phase shift is preferred to the IRS with non-equal phase shift.

However, the IRS with non-equal phase shift is capable of beamforming the reflected signal to the user in any desired direction through intelligent reflection. In this paper, the non-equal phase shift IRS and the equal phase shift IRS are both studied. Furthermore, considering the practical applications, we study both of the variable-height IRS and the fixed-height IRS. The variable-height IRS can be mounted on the aerial platforms such as balloons and UAVs while the fixed-height IRS can be installed on the indoor ceiling.

To the best of our knowledge, in the literature, there is only one existing work considering the alteration of IRS's position, i.e., [32]. In [32], a networking architecture is proposed that is enabled by aerial intelligent reflecting from the sky, where the transmit beamforming, IRS placement and phase shifts are jointly optimized. Instead of the free-space path loss channel model used in [32], we use the IRS-assisted wireless communication channel model that is based on the experimental results in [9]. Furthermore, we consider both of the variable-height IRS and the fixed-height IRS while the IRS is assumed to be placed at an altitude in [32].

We then optimize the IRS's position to achieve the maximum system rate. The main contributions of this paper are summarized in the following:

- We obtain a closed-form for the optimal IRS position that maximizes the system rate respectively for non-equal phase shift variable-height IRS, non-equal phase shift fixed-height IRS, equal phase shift variable-height IRS, and equal phase shift fixed-height IRS.
- We study all possibilities of the antenna directivity and show that the optimal position is directly related to different coefficients of the antenna directivity.
- Our analysis covers both cases of non-equal phase shift and equal phase shift IRS. The performance comparison provides quantitative insights on choosing the best suitable working mechanism for some specific setting.
- Considering the practical application, we study two different cases of IRS's height, i.e., the variable-height IRS and the fixed-height IRS.
- Our proposed results provide various insights on the optimal IRS position. For instance, our analysis provides the maximum possible height for the fixed-height IRS, which can not exceed a certain value.
- Simulations also reveal that the proposed optimal IRS's position outperforms any random IRS position in various settings.

The rest of the paper is organized as follows. In Section II, we describe the system model, the channel model, and formulation of the optimization problem. In Section III, we optimize the IRS's position for the non-equal phase shift variable-height IRS and the non-equal phase shift fixed-height IRS. In Section IV, we then design the position of the equal phase shift variable-height IRS and the equal phase shift fixed-height IRS. In Section V, the performance of the proposed optimal IRS's position is evaluated via simulation. Finally, in Section VI, we conclude the paper.

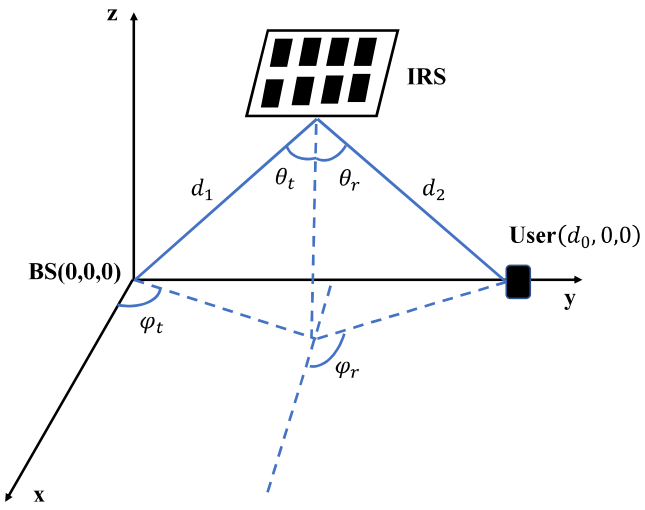

Figure 1. A schematic of the considered downlink IRS-assisted communications.

II. System Model

As shown in Fig.1, we consider an IRS-assisted communication system, wherein the base station (BS) equipped with single antenna communicates with the single antenna user through the IRS. Here, the user can be seen as a sensor, whose location is often fixed. It is assumed that there is no direct link between the IRS and the user. The first order reflection on the IRS is considered [13], [17], [33]. In addition, similar to [9], we focus on the scenario of far field, i.e., the distance between the BS and the user and the distance between the center of the IRS and the user are both larger than $\frac{2D^2}{\lambda}$, where D, and λ are the largest dimension of the IRS, and the wave length of the carrier signal respectively. Accordingly, the IRS's position is represented by the IRS's center. Moreover, the user is located at $(d_0, 0, 0)$ and the BS is located at $(0, 0, 0)$.

Let N, and M denote the number of the unit cells in the row and column of the IRS respectively. Each unit cell of the IRS is represented by $U_{n,m}$, for $n = 1, \cdots, N$, $m = 1, \cdots, M$. $\Theta_{n,m} = Ae^{j\phi_{n,m}}$ is the reflection coefficient of $U_{n,m}$ and the size of each $U_{n,m}$ is $d_n \times d_m$. In addition, in Fig. 1, d_1, d_2, θ_t, φ_t, θ_r and φ_r denote the distance between the BS and the center of the IRS, the distance between the user and the center of the IRS, the elevation angle and the azimuth angle from the BS to the center of the IRS, and the elevation angle and the azimuth angle from the center of the IRS to the user, respectively.

A. Channel Model

Suppose that s be the message intended to be received by the user with $E\left[|s|^2\right] = 1$. In the IRS-assisted communication system, the signal received at the user is [34]

$$y = \sqrt{P}\boldsymbol{h}_r\boldsymbol{\Theta}\boldsymbol{G}s + n = \sqrt{P}hs + n, \tag{1}$$

where P is the transmission power, $\boldsymbol{h}_r \in \mathbb{C}^{1\times MN}$, and $\boldsymbol{G} \in \mathbb{C}^{MN\times 1}$ are respectively the IRS-user link and the BS-IRS

link, and n is the additive white Gaussian noise (AWGN) at the user with zero mean and variance σ^2. In addition, $h = \boldsymbol{h}_r \boldsymbol{\Theta} \boldsymbol{G}$ denotes the channel coefficient from the BS to the user through the IRS. Similar to [9], we consider the following two cases for the far field scenario in the IRS-assisted communication channel.

1) Non-Equal Phase Shift: Each unit cell $U_{n,m}$ has non-equal phase shift, $\phi_{n,m}$, and the channel from the BS to the user through the IRS is

$$h_1 = \sqrt{\frac{G_t G_r G M^2 N^2 d_n d_m \lambda^2 f\left(\theta_t, \varphi_t\right) f\left(\theta_{des}, \varphi_{des}\right) A^2}{64\pi^3 d_1^2 d_2^2}}, \tag{2}$$

where $\theta_{des} = \theta_r$, $\varphi_{des} = \varphi_r$, and $(\theta_{des}, \varphi_{des})$ is the desired direction. In (2), the power radiation pattern is given by

$$f\left(\theta, \varphi\right) = \begin{cases} \cos^{\alpha}\theta, & 0 \le \theta \le \frac{\pi}{2}, 0 \le \varphi \le 2\pi, \\ 0, & \frac{\pi}{2} < \theta \le 2\pi, 0 \le \varphi \le 2\pi, \end{cases} \tag{3}$$

where $\alpha \ge 0$ represents the directivity of the antenna and a larger α implies a more focused beam or highly directional antenna [35]. In (2), G_t, G_r, and G denote antenna gains of the BS, the user, and the IRS, respectively. The proposed channel coefficient, h_1, is based on the non-equal phase shifts design in [9]

$$\begin{aligned} \phi_{n,m} &= \text{mod}\left(\frac{2\pi}{\lambda}\left(\delta_1\left(m-\frac{1}{2}\right)d_n + \delta_2\left(n-\frac{1}{2}\right)d_m\right), 2\pi\right) \\ &= \text{mod}\left(-\frac{2\pi\Psi}{\lambda}, 2\pi\right), \end{aligned} \tag{4}$$

where

$$\begin{aligned} \Psi =& (\sin\theta_t \cos\varphi_t + \sin\theta_{des}\cos\varphi_{des})\left(m-\frac{1}{2}\right)d_n \\ &+ (\sin\theta_t \sin\varphi_t + \sin\theta_{des}\sin\varphi_{des})\left(n-\frac{1}{2}\right)d_m. \end{aligned} \tag{5}$$

2) Equal Phase Shift: Secondly, each unit cell, $U_{n,m}$, has the equal phase shift, ϕ, the channel from the BS to the user through the IRS is

$$h_2 = \sqrt{\frac{G_t G_r G M^2 N^2 d_n d_m \lambda^2 f\left(\theta, \varphi\right) f\left(\theta, \varphi+\pi\right) A^2}{64\pi^3 d_1^2 d_2^2}}, \tag{6}$$

where $\theta = \theta_r = \theta_t$, $\varphi = \varphi_t$, and the power radiation pattern is as in (3). Note that, for the equal phase shift IRS, h_2 can be obtained by any random phase shift. Hence, considering the production costs, the equal phase shift IRS is more preferred compared to the non-equal phase shift IRS.

B. Achieved Rate Maximization

In this paper, with the fixed BS's and user's locations, by optimizing IRS's location, i.e., optimizing θ_t, φ_t, θ_r, and φ_r, the channel gains can be reconfigured for obtaining further improvements in the system performance. In other words, employing the IRS, one can reconfigure the propagation environment, which could greatly improve the system performance, see, e.g., [17], [31]. In the current literature, however, the position of the IRS is always assumed fixed. Assuming movability of the IRS provides an extra degree of freedom to improve system efficiency. Here, we focus on an IRS-assisted communication system, where the IRS is assumed to be movable. We analysis far field scenario where $d_0 \ge \frac{2D^2}{\lambda}$ [9].

In the considered setting, the IRS's position can be freely moved to achieve the best performance. In addition, the IRS's position can also be designed based on the settings of the environment, e.g., existing building. The IRS can be installed on the ceiling, which has the fixed height. In this paper, for different channel models in (2) and (6), we investigate the optimization of the IRS's position for two cases including the variable-height IRS, and the fixed-height IRS.

1) The Variable-Height IRS: In this case, from Fig.1, we write

$$d_1 \cos\theta_t = d_2 \cos\theta_r, \tag{7}$$

$$d_1 \sin\theta_t \left|\sin\varphi_t\right| + d_2 \sin\theta_r \left|\sin\varphi_r\right| = d_0, \tag{8}$$

$$d_1 \sin\theta_t \left|\cos\varphi_t\right| = d_2 \sin\theta_r \left|\cos\varphi_r\right|. \tag{9}$$

Using (7) and (8), we then obtain:

$$d_1 = \frac{d_0 \cos\theta_r}{\sin\theta_t \cos\theta_r \left|\sin\varphi_t\right| + \sin\theta_r \cos\theta_t \left|\sin\varphi_r\right|}, \tag{10}$$

$$d_2 = \frac{d_0 \cos\theta_t}{\sin\theta_t \cos\theta_r \left|\sin\varphi_t\right| + \sin\theta_r \cos\theta_t \left|\sin\varphi_r\right|}. \tag{11}$$

Hence, the position of the IRS can be fully represented by the variables, θ_t, φ_t, θ_r, and φ_r. The channel models provided in (2) and (6) are also functions of variables θ_t, φ_t, θ_r, and φ_r.

Here, our objective is to find the optimal IRS position, so that the user's achieved rate is maximized:

$$\max_{\{\theta_t, \varphi_t, \theta_r, \varphi_r\}} R = \log\left(1 + \frac{Ph^2}{\sigma^2}\right), \tag{12}$$

$$\text{s.t. } d_1, d_2 \ge \frac{2D^2}{\lambda}, \tag{13}$$

$$d_1 \sin\theta_t \left|\cos\varphi_t\right| = d_2 \sin\theta_r \left|\cos\varphi_r\right|, \tag{14}$$

$$0 \le \varphi_t, \varphi_r \le 2\pi, \tag{15}$$

$$0 \le \theta_t, \theta_r \le \frac{\pi}{2}. \tag{16}$$

In the above optimization problem (12), (13) ensures the far field assumption and (14) represents the intrinsic geometric characteristic (9) in Fig.1. Furthermore, (15) and (16) ensures that the azimuth angles, i.e., φ_t and φ_r, are within $[0, 2\pi]$, while the elevation angles, i.e., θ_t and θ_r, are assumed to be within $\left[0, \frac{\pi}{2}\right]$. This enforces $f\left(\theta, \varphi\right) = 0$, $\frac{\pi}{2} < \theta \le 2\pi$, i.e., the power radiation pattern function.

2) The Fixed-Height IRS: In this case, the height is fixed at H. Using Fig.1, we write.

$$d_1 = \frac{\mathrm{H}}{\cos\theta_t}, \tag{17}$$

$$d_2 = \frac{\mathrm{H}}{\cos\theta_r}. \tag{18}$$

In this case, the IRS's position is fully represented by the variables θ_t, φ_t, θ_r, and φ_r and similar to (12), the rate maximization problem is formulated as

$$\max_{\{\theta_t,\varphi_t,\theta_r,\varphi_r\}} R = \log\left(1+\frac{Ph^2}{\sigma^2}\right), \tag{19}$$

$$\text{s.t. } d_1, d_2 \geq \frac{2D^2}{\lambda}, \tag{20}$$

$$\frac{H}{\cos\theta_t}\sin\theta_t\left|\cos\varphi_t\right| = \frac{H}{\cos\theta_r}\sin\theta_r\left|\cos\varphi_r\right|, \tag{21}$$

$$\frac{H}{\cos\theta_t}\sin\theta_t\left|\sin\varphi_t\right| + \frac{H}{\cos\theta_r}\sin\theta_r\left|\sin\varphi_r\right| = d_0, \tag{22}$$

$$0 \leq \varphi_t, \varphi_r \leq 2\pi, \tag{23}$$

$$0 \leq \theta_t, \theta_r \leq \frac{\pi}{2}, \tag{24}$$

where the constraints (21) and (22) represent the intrinsic geometric characteristic as seen in Fig. 1 and (20), (23), and (24) are similar to (13), (15), and (16).

In this paper, we find solutions to problem (12) and (19) for two different channel models, i.e., the channel model for non-equal phase shift as in (2), and the channel model for the equal phase shift as in (6). The complex form of the channel gains, however, challenges the optimization of IRS's position. In the following, we obtain the optimal IRS's position for different cases of phase shift, and height.

III. Optimization of the IRS Position: Non-Equal Phase Shift

Here, we obtain the optimal IRS's position for maximizing the system achieved rate for the variable-height IRS and the fixed-height IRS, where each unit cell $U_{n,m}$ has a different reflecting coefficient, $\Theta_{n,m} = Ae^{j\phi_{n,m}}$.

A. The Non-Equal Phase Shift Variable-Height (NE-VH) IRS

Adopting the channel model (2), problem in (12) is equivalent to the following optimization problem:

$$\max_{\{\theta_t,\varphi_t,\theta_{des},\varphi_{des}\}} g_1\left(\theta_t,\varphi_t,\theta_{\text{des}},\varphi_{\text{des}}\right), \tag{25}$$

$$\text{s.t. } \cos\theta_{des} - \iota\Omega \geq 0, \tag{26}$$

$$\cos\theta_t - \iota\Omega \geq 0, \tag{27}$$

$$\cos\theta_{\text{des}}\sin\theta_t\left|\cos\varphi_t\right| = \cos\theta_t\sin\theta_{\text{des}}\left|\cos\varphi_{\text{des}}\right|, \tag{28}$$

$$0 \leq \varphi_t, \varphi_r \leq 2\pi, \tag{29}$$

$$0 \leq \theta_t, \theta_r \leq \frac{\pi}{2}, \tag{30}$$

where

$$\Omega = \sin\theta_t\cos\theta_{\text{des}}\left|\sin\varphi_t\right| + \sin\theta_{\text{des}}\cos\theta_t\left|\sin\varphi_{des}\right|, \tag{31}$$

and $\iota = \frac{2D^2}{\lambda d_0} \leq 1$. In problem (25), the objective function is written as

$$g_1\left(\theta_t,\varphi_t,\theta_{\text{des}},\varphi_{\text{des}}\right) = \frac{\Gamma\cos^{\alpha}\theta_t\cos^{\alpha}\theta_{\text{des}}}{d_1^2 d_2^2} = \frac{\Gamma\cos^{\alpha-2}\theta_t\cos^{\alpha-2}\theta_{\text{des}}\Omega^4}{d_0^4}, \tag{32}$$

where

$$\Gamma = \frac{G_t G_r G M^2 N^2 d_x d_y \lambda^2 A^2}{64\pi^3}. \tag{33}$$

In order to solve problem (25), we propose a change of variable by defining the new variables $t_1 = |\sin\varphi_t|$ and $t_2 = |\sin\varphi_{\text{des}}|$, which satisfy $0 \leq t_1 \leq 1$, and $0 \leq t_2 \leq 1$. We then optimize t_1 and t_2 by fixing θ_t and θ_{des}. The corresponding optimization problem is reduced to

$$\max_{t_1,t_2} \frac{\Gamma\cos^{\alpha-2}\theta_t\cos^{\alpha-2}\theta_{\text{des}}(t_1\sin\theta_t\cos\theta_{\text{des}}+t_2\sin\theta_{\text{des}}\cos\theta_t)^4}{d_0^4}, \tag{34}$$

$$\text{s.t. } \cos\theta_{\text{des}} - \iota\left(t_1\sin\theta_t\cos\theta_{\text{des}} + t_2\sin\theta_{\text{des}}\cos\theta_t\right) \geq 0, \tag{35}$$

$$\cos\theta_t - \iota\left(t_1\sin\theta_t\cos\theta_{\text{des}} + t_2\sin\theta_{\text{des}}\cos\theta_t\right) \geq 0, \tag{36}$$

$$\cos\theta_{\text{des}}\sin\theta_t\sqrt{1-t_1^2} = \cos\theta_t\sin\theta_{\text{des}}\sqrt{1-t_2^2}, \tag{37}$$

$$0 \leq t_1, t_2 \leq 1. \tag{38}$$

In the following Proposition, we provide the optimal solution to (34).

Proposition 1. *The optimal solution to problem* (34) *is* $t_1^* = 1,\ t_2^* = 1$.

Proof. See Appendix A. □

Remark 1. According to Proposition 1, the optimal φ_t^* and φ_{des}^* satisfy $|\sin\varphi_t^*| = |\sin\varphi_{\text{des}}^*| = 1$, i.e., $\varphi_t^* = \frac{\pi}{2}$ or $\varphi_t^* = \frac{3\pi}{2}$, $\varphi_{\text{des}}^* = \frac{\pi}{2}$ or $\varphi_{\text{des}}^* = \frac{3\pi}{2}$. Hence, the optimal position of the NE-VH IRS is always on the vertical plane.

Using the optimal values of φ_t and φ_{des}, we then optimize θ_t and θ_{des}. The corresponding optimizing problem is

$$\max_{\theta_t,\theta_{\text{des}}} \frac{\Gamma\cos^{\alpha-2}\theta_t\cos^{\alpha-2}\theta_{\text{des}}\sin^4(\theta_t+\theta_{\text{des}})}{d_0^4}, \tag{39}$$

$$\text{s.t. } \cos\theta_{\text{des}} - \iota\sin(\theta_t+\theta_{\text{des}}) \geq 0, \tag{40}$$

$$\cos\theta_t - \iota\sin(\theta_t+\theta_{\text{des}}) \geq 0, \tag{41}$$

$$0 \leq \theta_t, \theta_{\text{des}} \leq \frac{\pi}{2}. \tag{42}$$

The optimization problem in (39) is non-convex due to the non-concave objective function. In the following Theorem, we provide the optimal solution to problem (39).

Theorem 1. *The optimal solution to problem* (39) *is*

$$0 \le \alpha < 2 : \theta_t^* = \Upsilon^* - \arccos\left(\iota \sin \Upsilon^*\right), \tag{43}$$
$$\theta_{des}^* = \arccos\left(\iota \sin \Upsilon^*\right), \text{ or}$$
$$\theta_t^* = \arccos\left(\iota \sin \Upsilon^*\right), \tag{44}$$
$$\theta_{des}^* = \Upsilon^* - \arccos\left(\iota \sin \Upsilon^*\right),$$
$$\alpha = 2 : \begin{cases} \theta_t^* = \theta_{des}^* = \arcsin \frac{1}{2\iota}, & \frac{1}{2\iota} \le 1, \\ \theta_t^*, \theta_{des}^* = \mathbb{A}, & \frac{1}{2\iota} > 1, \end{cases} \tag{45}$$
$$\alpha > 2 : \theta_t^* = \theta_{des}^* = \begin{cases} \arccos\left(\sqrt{\frac{\alpha}{\alpha+2}}\right), & \frac{1}{4\iota^2} \ge \frac{2}{\alpha+2}, \\ \arccos\left(\sqrt{1-\frac{1}{4\iota^2}}\right), & \frac{1}{4\iota^2} < \frac{2}{\alpha+2}, \end{cases} \tag{46}$$

where in the above,

$$\mathbb{A} = \left\{\theta_t^*, \theta_{des}^* \mid \theta_t^* + \theta_{des}^* = \frac{\pi}{2}, \frac{\pi}{2} - \arccos\iota \le \theta_t^* \le \arccos\iota\right\}, \tag{47}$$

$$\Upsilon^* = \arcsin\left(\frac{\cos\nu}{\sqrt{1+\iota^2-2\iota\sin\nu}}\right), \tag{48}$$

$$\nu = \begin{cases} 0, & \Xi < 0, \\ \Xi, & 0 \le \Xi \le \arcsin\min\left\{\frac{1}{2\iota}, 1\right\}, \\ \arcsin\min\left\{\frac{1}{2\iota}, 1\right\}, & \Xi > \arcsin\min\left\{\frac{1}{2\iota}, 1\right\}, \end{cases} \tag{49}$$

and

$$\Xi = \begin{cases} \arcsin\left(\frac{\alpha\left(1+\iota^2\right)-\sqrt{(1+\iota^4-\iota^2)\alpha^2-4\iota^2\alpha+4\iota^2}}{(3\alpha\iota-2\iota)}\right), & \alpha \ne \frac{2}{3}, \\ \arcsin\left(\frac{2\iota}{(1+\iota^2)}\right), & \alpha = \frac{2}{3}. \end{cases} \tag{50}$$

Proof. See Appendix B. □

Remark 2. According to Theorem 1, for the NE-VH IRS, the optimal elevation angles are characterized with three cases, i.e., $0 \le \alpha < 2$, $\alpha = 2$, and $\alpha > 2$. Specifically, if $0 \le \alpha < 2$, the optimal elevation angles, i.e., θ_t^* and θ_{des}^*, always take different values. Given $\alpha = 2$ and $\frac{1}{2\iota} > 1$, to achieve the best performance, the optimal elevation angles can have various choices. In addition, the optimal elevation angles are always equal for $\alpha > 2$. Furthermore, if $\frac{1}{4\iota^2} < \frac{2}{\alpha+2}$ and $\alpha > 2$, the optimal elevation angles are $\theta_t^* = \theta_{\text{des}}^* = \arccos\left(\sqrt{1-\frac{1}{4\iota^2}}\right)$.

Consequently, the optimal position for the NE-VH IRS is jointly characterized by Proposition 1 and Theorem 1. The optimal three-dimensional coordinates of the NE-VH IRS are given by

$$(L_x, L_y, L_z) = \left(0, r_1 \sin\theta_t^*, r_1 \cos\theta_t^*\right), \tag{51}$$

where

$$r_1 = \frac{d_0 \cos\theta_r^*}{\sin\theta_t^* \cos\theta_r^* + \sin\theta_r^* \cos\theta_t^*}. \tag{52}$$

Furthermore, using the proposed optimal azimuth angles and elevation angles, the corresponding optimal phase shift, $\phi_{n,m}$, for $n = 1, \cdots, N$, $m = 1, \cdots, M$ of the NE-VH IRS are given by (4).

B. The Non-Equal Phase Shift Fixed-Height (NE-FH) IRS

In this subsection, given the fixed height of the IRS, its position is optimized to maximize the user's achieved rate. Adopting the channel model proposed in (2), the optimization problem (19) is transformed to the following form:

$$\max_{\{\theta_t, \varphi_t, \theta_{\text{des}}, \varphi_{\text{des}}\}} g_2\left(\theta_t, \varphi_t, \theta_{\text{des}}, \varphi_{\text{des}}\right), \tag{53}$$
$$\text{s.t. } \frac{H}{\cos\theta_t} \ge \frac{2D^2}{\lambda}, \tag{54}$$
$$\frac{H}{\cos\theta_{\text{des}}} \ge \frac{2D^2}{\lambda}, \tag{55}$$
$$\frac{H}{\cos\theta_t} \sin\theta_t \left|\cos\varphi_t\right| \tag{56}$$
$$= \frac{H}{\cos\theta_{\text{des}}} \sin\theta_{\text{des}} \left|\cos\varphi_{\text{des}}\right|,$$
$$\frac{H}{\cos\theta_t} \sin\theta_t \left|\sin\varphi_t\right| \tag{57}$$
$$+ \frac{H}{\cos\theta_{\text{des}}} \sin\theta_{\text{des}} \left|\sin\varphi_{\text{des}}\right| = d_0,$$
$$0 \le \varphi_t, \varphi_{\text{des}} \le 2\pi, \tag{58}$$
$$0 \le \theta_t, \theta_{\text{des}} \le \frac{\pi}{2}, \tag{59}$$

where the objective function in (53) is

$$g_2\left(\theta_t, \varphi_t, \theta_{\text{des}}, \varphi_{\text{des}}\right) = \frac{\Gamma \cos^{\alpha}\theta_t \cos^{\alpha}\theta_{\text{des}}}{d_1^2 d_2^2}, \tag{60}$$
$$= \frac{\Gamma \cos^{\alpha+2}\theta_t \cos^{\alpha+2}\theta_{\text{des}}}{\mathrm{H}^4}.$$

In order to solve problem (53), we first optimize the azimuth angles, i.e., φ_t and φ_{des}, by fixing the elevation angles, i.e., θ_t and θ_{des}. The solution of the azimuth angles is given in the following Proposition.

Proposition 2. *In* (53)*, given θ_t and θ_{des}, the optimal azimuth angles φ_t^* and φ_{des}^* are*

$$\varphi_t^* = \varphi_{FHt}^* = \arcsin\Omega_1, \text{ or } \varphi_t^* = \varphi_{FHt}^* = \arcsin\Omega_1 + \pi, \tag{61}$$

$$\varphi_{des}^* = \varphi_{FHdes}^* = \arcsin\Omega_2, \text{ or } \varphi_{des}^* = \varphi_{FHdes}^* = \arcsin\Omega_2 + \pi, \tag{62}$$

where

$$\Omega_1 = \frac{\tan^2\theta_t - \tan^2\theta_{des} + \frac{d_0^2}{H^2}}{2\frac{d_0}{H}\tan\theta_t}, \tag{63}$$

$$\Omega_2 = \frac{\tan^2\theta_{des} - \tan^2\theta_t + \frac{d_0^2}{H^2}}{2\frac{d_0}{H}\tan\theta_{des}}. \tag{64}$$

Proof. See Appendix C. □

As it is seen in Proposition 2, in contrast to the NE-VH IRS, the azimuth angles of the NE-FH IRS are determined by the elevation angles, the height, and the distance of the user from the BS.

By using the results provided in Proposition 2, we further optimize the elevation angles θ_t and θ_{des}. Using the following optimization problem:

$$\max_{\theta_t,\theta_{\text{des}}} \frac{\Gamma \cos^{\alpha+2}\theta_t \cos^{\alpha+2}\theta_{\text{des}}}{H^4}, \tag{65}$$

$$\text{s.t. } \frac{H}{\cos\theta_t} \geq \frac{2D^2}{\lambda}, \tag{66}$$

$$\frac{H}{\cos\theta_{\text{des}}} \geq \frac{2D^2}{\lambda}, \tag{67}$$

$$0 \leq \theta_t, \theta_{\text{des}} \leq \frac{\pi}{2}. \tag{68}$$

The above optimal optimization problem is nonconvex as the objective function in (65) is not concave. The following Theorem provides the solutions.

Theorem 2. *The optimal solution to problem* (65) *is*

$$\theta_t^* = \theta_{des}^* = \theta_{FH}^* = \arccos\Delta, \tag{69}$$

where

$$\Delta = \min\left\{\frac{H\lambda}{2D^2}, 1\right\}. \tag{70}$$

Proof. See Appendix D. □

Remark 3. Theorem 2 indicates that the optimal elevation angles for the NE-FH IRS are always equal. In addition, the optimal elevation angles for the NE-FH IRS are determined by the height, H, and are not related to the antenna directivity. Specifically, as expected, if $H \leq \frac{2D^2}{\lambda}$, the elevation angles decrease by increasing H. However, if the height is large enough to satisfy $H > \frac{2D^2}{\lambda}$, the optimal elevation angles are $\theta_{\text{des}}^* = \theta_t^* = 0$, which is in fact the extreme case.

The optimal position of the NE-FH IRS for maximizing rate is fully characterized by Proposition 2 and Theorem 2, i.e., the three-dimensional position is given by

$$(L_x, L_y, L_z) = (H\tan\theta_{\text{FH}}^*\cos\varphi_{\text{FHt}}^*, H\tan\theta_{\text{FH}}^*\sin\varphi_{\text{FHt}}^*, H). \tag{71}$$

In addition, the optimal phase shifts of the NE-FH IRS are obtained by setting $\theta_t^* = \theta_{\text{des}}^* = \theta_{\text{FH}}^*$, $\varphi_t^* = \varphi_{\text{FHt}}^*$, and $\varphi_{\text{des}}^* = \varphi_{\text{FHdes}}^*$ in (4).

IV. Optimization of the IRS's Position: Equal Phase Shift

Here, we investigate the cases when the IRS shares the same reflecting coefficient, i.e., $\Theta_{n,m} = Ae^{j\phi}$, for $n = 1,\cdots,N$, $m = 1,\cdots,M$. According to (6), the optimal elevation angles and the azimuth angles for the equal phase shift IRS shall satisfy $\theta_r = \theta_t$ and $\varphi_r = \varphi_t + \pi$, respectively, and the corresponding optimal phase shift, i.e., Φ, can take any value. Similarly, in the following, we obtain the optimal IRS's position for the variable-height IRS and the fixed-height IRS, respectively.

A. Equal Phase Shift Variable-Height (E-VH) IRS

Using (10), (11), $\theta_r = \theta_t$, and $\varphi_r = \varphi_t + \pi$, therefore

$$d_1 = d_2 = \frac{d_0}{2\sin\theta\,|\sin\varphi|}, \tag{72}$$

where $\theta = \theta_r = \theta_t$ and $\varphi = \varphi_t$. Therefore, the optimization problem in (12) is reduced to

$$\max_{\theta,\varphi} v_1(\theta,\varphi) = \frac{16\Gamma}{d_0^4}\cos^{2\alpha}\theta\sin^4\theta\sin^4\varphi, \tag{73}$$

$$\text{s.t. } \frac{d_0}{2\sin\theta\,|\sin\varphi|} \geq \frac{2D^2}{\lambda}, \tag{74}$$

$$0 \leq \theta \leq \frac{\pi}{2}, \tag{75}$$

$$0 \leq \varphi \leq 2\pi. \tag{76}$$

Similar to the above, the objective function in (73) results in non-convexity of the optimization problem. The following Theorem provides the closed-form optimal solution to problem (73).

Theorem 3. *The optimal solution to problem* (73) *is given by*

$$\theta^* = \begin{cases} \arccos\left(\sqrt{\frac{\alpha}{\alpha+2}}\right), & \frac{1}{4\iota^2} \geq \frac{2}{\alpha+2}, \\ \arccos\left(\sqrt{1-\frac{1}{4\iota^2}}\right), & \frac{1}{4\iota^2} < \frac{2}{\alpha+2}, \end{cases} \tag{77}$$

$$\varphi^* = \frac{\pi}{2} \text{ or } \frac{3\pi}{2}.$$

Proof. See Appendix E. □

Remark 4. According to Theorem 3, the optimal azimuth angles of the E-VH IRS are given by $\varphi_r^* = \varphi^* = \frac{\pi}{2}$ or $\frac{3\pi}{2}$ and $\varphi_{\text{des}} = \varphi^* + \pi$, which are same as the NE-VH IRS. In addition, given $\alpha > 2$, the optimal elevation angles are also the same as NE-VH IRS. It is also seen the optimal elevation angles decrease by increasing α. This is because the increasing of α means higher directivity. Thus the optimal elevation angles decrease to achieve a higher performance.

Therefore, the optimal position of the E-VH IRS to maximize the achieved rate is obtained by using Theorem 3 as

$$(L_x, L_y, L_z) = (0, r_2\sin\theta^*, r_2\cos\theta^*), \tag{78}$$

where $r_2 = \frac{d_0}{2\sin\theta^*}$.

B. Equal Phase Shift Fixed-Height (E-FH) IRS

In this subsection, we focus on the E-FH IRS and the height of the IRS is fixed at Hm. In Fig.1, we have

$$d_1 = d_2 = \frac{H}{\cos\theta}, \tag{79}$$

and

$$\frac{2H}{\cos\theta}\sin\theta\,|\sin\varphi| = d_0, \tag{80}$$

where $\theta = \theta_r = \theta_t$ and $\varphi = \varphi_t$. Hence, the rate maximization problem in (19) is transformed to the following:

$$\max_{\{\theta,\varphi\}} \; v_2(\theta,\varphi) = \frac{\Gamma \cos^{4+2\alpha}\theta}{H^4}, \tag{81}$$

$$\text{s.t.} \; \frac{H}{\cos\theta} \geq \frac{2D^2}{\lambda}, \tag{82}$$

$$\frac{2H}{\cos\theta}\sin\theta\,|\sin\varphi| = d_0, \tag{83}$$

$$0 \leq \varphi \leq 2\pi, \tag{84}$$

$$0 \leq \theta \leq \frac{\pi}{2}. \tag{85}$$

The optimal solution to problem (81) is given in the following Theorem.

Theorem 4. *The optimal solution to problem* (81) *is*

$$\theta^* = \theta^*_{FH} = \arccos\min\left\{\frac{H\lambda}{2D^2}, 1\right\}, \tag{86}$$

$$\varphi^* = \varphi^*_{FH} = \Xi \text{ or } \varphi^* = \varphi^*_{FH} = \Xi + \pi, \tag{87}$$

where

$$\Xi = \arcsin\frac{d_0}{2H\tan\theta^*_{FH}}. \tag{88}$$

Proof. See Appendix F. □

Remark 5. From Theorem 4, it is easy to find out that the optimal azimuth and elevation angles of the E-FH IRS are the same as the NE-FH IRS. The optimal azimuth angles and elevation angles are also not affected by the value of α. Therefore, the antenna directivity has no effect on the optimal position.

Thereby, the optimal position of the E-FH IRS for the rate maximization is provided by Theorem 4 as the following

$$(L_x, L_y, L_z) = \left(H\tan\theta^*_{\text{FH}}\cos\varphi^*_{\text{FH}}, H\tan\theta^*_{\text{FH}}\sin\varphi^*_{\text{FH}}, H\right). \tag{89}$$

V. Simulation Result

In this section, we show the performance of our proposed solution to the rate maximization problem in the downlink IRS-assisted communication system. According to [35], by assuming 100% antenna efficiency, the antenna gain is

$$G_{antenna} = \frac{4\pi}{\int_{\varphi=0}^{2\pi}\int_{\theta=0}^{\pi} F(\theta,\varphi)\sin\theta \mathrm{d}\theta\mathrm{d}\varphi}, \tag{90}$$

where $F(\theta,\varphi)$ is the normalized power radiation pattern. In our simulations, using $F_t(\theta_t,\varphi_t) = F_r(\theta_r,\varphi_r) = 1$, $F(\theta,\varphi) = f(\theta,\varphi)$, we easily obtain G_t, G_r, and G. The other parameters of the IRS are given by $M = N = 100$, $d_n = d_m = 0.01$, $A = 0.9$, operating frequency, $f = 10.5$GHz, $\lambda = c/f = 0.0286$m, and $\frac{2D^2}{\lambda} = \frac{2MNd_xd_y}{\lambda} = 71.4$m [9]. The bandwidth is $B = 10$MHz. The noise power is $\sigma^2 = BN_0$ with $N_0 = -174$dBm. The transmission power of the BS is $P = 10$W.

In the following, we will evaluate the system performance using the IRS with different cases of phase shifts and heights. The proposed optimal positions are then compared with the random positions for different antenna directivity, α, and distances from the user to the BS, d_0. In addition, in our simulations, the fixed-height (FH) IRS represents both of the E-FH IRS and the NE-FH IRS, as it is seen the E-FH IRS and the NE-FH IRS achieve the same performance.

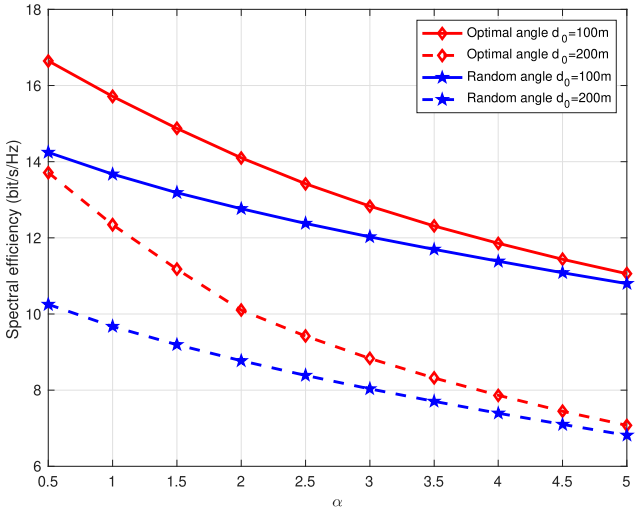

Figure 2. The spectral efficiency versus α for the NE-VH IRS.

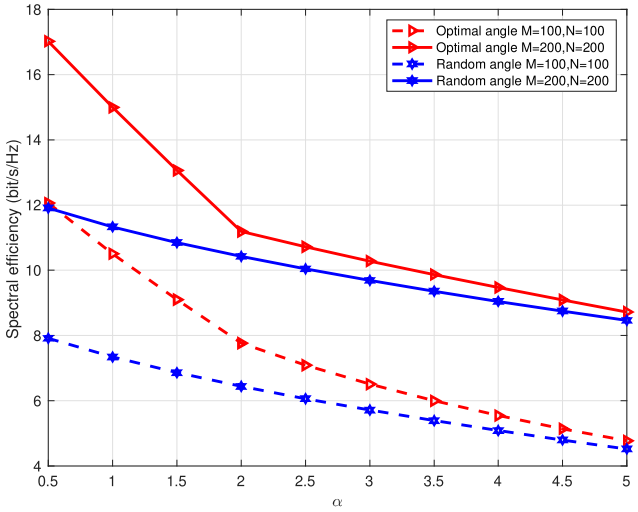

Figure 3. The spectral efficiency versus α for the NE-VH IRS.

In Figs. 2. 3, we show the data rate achieved by our proposed optimal position for the NE-VH IRS. As seen from the figure, our proposed optimal position outperforms the random position. The performance gap between the schemes with the proposed optimal position and the random position is increased with smaller α and d_0. In addition, increasing α results in a significant decrease of the rate performance, especially for small values of α. Furthermore, from Fig. 3, it's easy to find that the system performance can be obviously improved by increasing the number of IRS units.

Fig. 4 depicts the comparison between the NE-VH IRS and

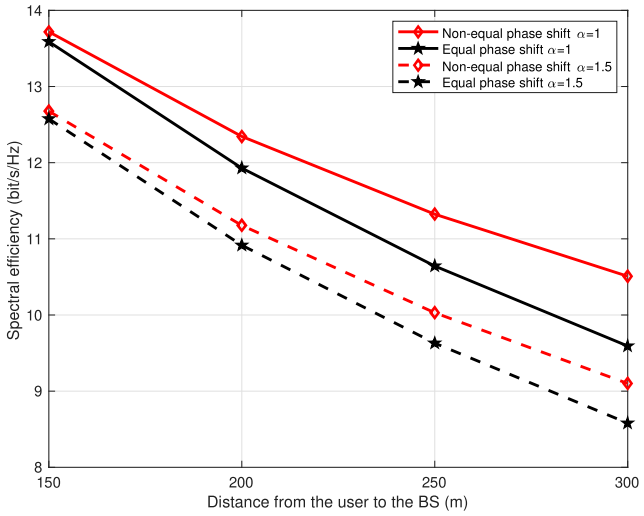

Figure 4. The spectral efficiency versus the distance from the user to the BS for the HF IRS.

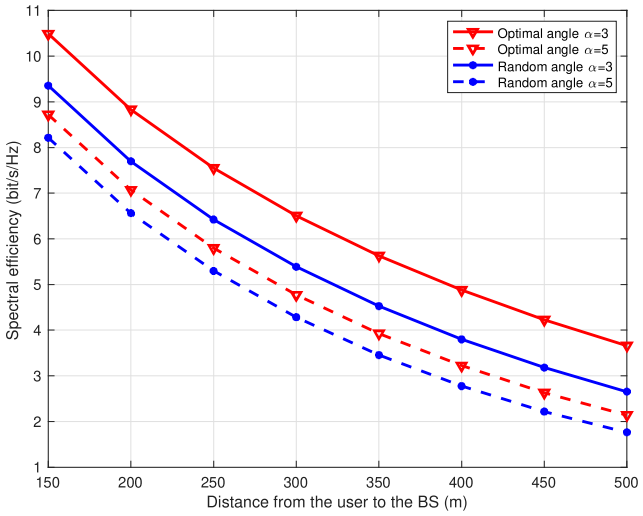

Figure 5. The spectral efficiency versus the distance from the user to the BS for the VH IRS.

the E-VH IRS. It is clearly seen that the NE-VH IRS achieves better rate performance than that of the E-VH IRS, which is because the NE-VH IRS is able to beamform the reflected signal toward the user in any desired direction via intelligent reflection. Furthermore, increasing d_0 results in decreasing the performance gap while there is a larger gap between the NE-VH IRS and the E-VH IRS by reducing α. Considering practical issues such as production cost, the above results suggest that NE-VH IRS is preferred to E-VH IRS for $\alpha > 2$ and large d_0.

Fig. 5 shows the spectral efficiency versus the distance from the user to the BS for the variable-height (VH) IRS. According to Theorem 1 and Theorem 3, given $\alpha > 2$, the NE-VH IRS and the E-VH IRS achieve the same rate performance. Thus, the results in Fig. 4 are for the VH IRS. As it is seen the proposed optimal position achieves a higher performance than that of the random position. Furthermore, the performance improvement is more obvious significant for a smaller α and d_0.

Figs. 6. 7 demonstrate the spectral efficiency performance versus the height, and α for the fixed-height (FH) IRS respectively. Similar trend is seen as in Fig. 4 and Fig. 2, where our proposed position scheme outperforms the random position. In addition, the gap is much larger with larger values of α. However, different from Fig. 4 and Fig. 2, the performance gap almost keeps same for different values of H.

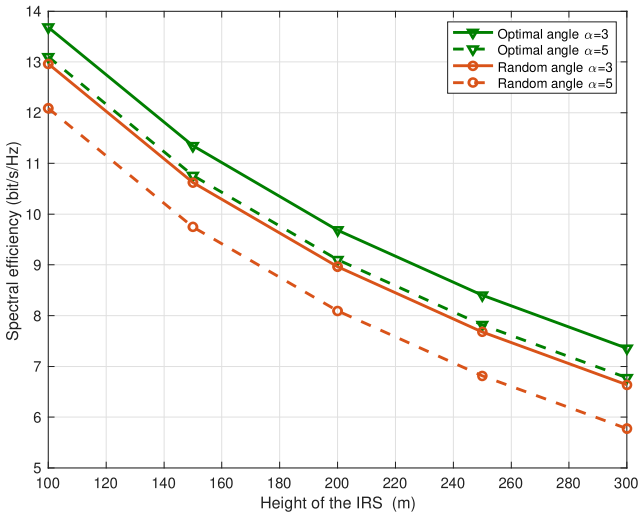

Figure 6. The spectral efficiency versus the height for the FH IRS.

VI. Conclusion

In this paper, we have studied the optimization of IRS's position in the IRS-assisted communication system to maximize the system rate. Considering the practical application, the cases of equal phase shift and non-equal phase shift and the cases of free height and fixed height are all studied. The optimal IRS's 3D position has been characterized in closed forms respectively for the NE-VH IRS, the NE-FH IRS, the E-VH IRS, and the E-FH IRS. Moreover, we considered all possibilities of the directivity of antenna and showed that the IRS's position is closely related to the directivity coefficient. We also provided a lot of insights about the influence factors of the optimal solution, which is instructive to the practical application. The simulation results have shown that the proposed optimal IRS's position achieves better performance than any random location.

Appendix

A. Proof of Proposition 1

Problem (34) is difficult to solve due to the equality constraint in (37). We first relax this constraint, reduce problem

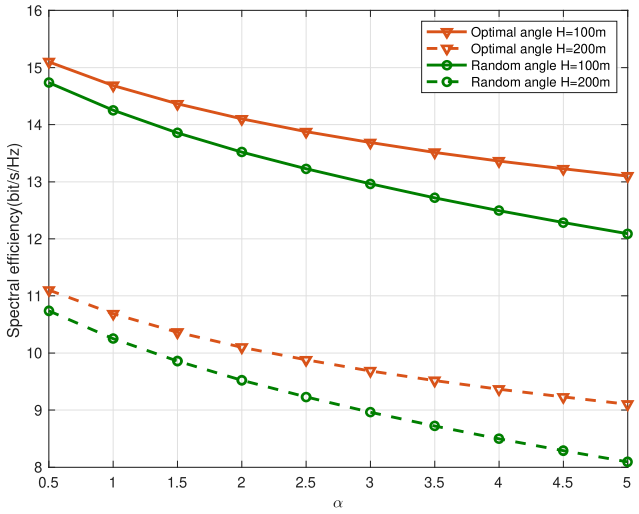

Figure 7. The spectral efficiency versus α for the FH IRS.

(34) to

$$\max_{t_1,t_2} \; t_1 \sin\theta_t \cos\theta_{\text{des}} + t_2 \sin\theta_{\text{des}} \cos\theta_t, \tag{91}$$
$$\text{s.t.} \;\; \cos\theta_{\text{des}} - \iota\left(t_1 \sin\theta_t \cos\theta_{\text{des}} + t_2 \sin\theta_{\text{des}} \cos\theta_t\right) \geq 0,$$
$$\cos\theta_t - \iota\left(t_1 \sin\theta_t \cos\theta_{\text{des}} + t_2 \sin\theta_{\text{des}} \cos\theta_t\right) \geq 0,$$
$$0 \leq t_1, t_2 \leq 1,$$

which is a convex optimization problem. Using Lagrange coefficients methods, we get

$$\begin{aligned} L =& t_1 \sin\theta_t \cos\theta_{\text{des}} + t_2 \sin\theta_{\text{des}} \cos\theta_t \\ &+ \mu_1\left(\cos\theta_{\text{des}} - \iota\left(t_1 \sin\theta_t \cos\theta_{\text{des}} + t_2 \sin\theta_{\text{des}} \cos\theta_t\right)\right) \\ &+ \mu_2\left(\cos\theta_t - \iota\left(t_1 \sin\theta_t \cos\theta_{\text{des}} + t_2 \sin\theta_{\text{des}} \cos\theta_t\right)\right) \\ &- \mu_3\left(t_1 - 1\right) - \mu_4\left(t_2 - 1\right), \end{aligned}$$

where μ_1, μ_2, μ_3, and μ_4 are the Lagrange multipliers. As (91) is a convex optimization problem, its optimal solution is characterized by the following Karush-Kuhn-Tucker (KKT) [36] conditions:

$$\frac{\partial L}{\partial t_1} = \sin\theta_t \cos\theta_{\text{des}} - \mu_1 \iota \sin\theta_t \cos\theta_{\text{des}} - \mu_2 \iota \sin\theta_t \cos\theta_{\text{des}} - \mu_3 = 0, \tag{92}$$

$$\frac{\partial L}{\partial t_2} = \sin\theta_{\text{des}} \cos\theta_t - \mu_1 \iota \sin\theta_{\text{des}} \cos\theta_t - \mu_2 \iota \sin\theta_{\text{des}} \cos\theta_t - \mu_4 = 0, \tag{93}$$

$$\mu_1\left(\cos\theta_t - \iota\left(t_1 \sin\theta_t \cos\theta_{\text{des}} + t_2 \sin\theta_{\text{des}} \cos\theta_t\right)\right) = 0, \tag{94}$$

$$\mu_2\left(\cos\theta_{\text{des}} - \iota\left(t_1 \sin\theta_t \cos\theta_{\text{des}} + t_2 \sin\theta_{\text{des}} \cos\theta_t\right)\right) = 0, \tag{95}$$

$$\mu_3\left(t_1 - 1\right) = 0, \tag{96}$$

$$\mu_4\left(t_2 - 1\right) = 0. \tag{97}$$

From the KKT conditions, five cases should be considered, which are respectively (1) $\mu_1 = 0$, $\mu_2 = 0$, $\mu_3 \neq 0$, $\mu_4 \neq 0$; (2) $\mu_1 = 0$, $\mu_2 \neq 0$, $\mu_3 \neq 0$, $\mu_4 = 0$; (3) $\mu_1 = 0$, $\mu_2 \neq 0$, $\mu_3 = 0$, $\mu_4 \neq 0$; (4) $\mu_1 \neq 0$, $\mu_2 = 0$, $\mu_3 \neq 0$, $\mu_4 = 0$; (5) $\mu_1 \neq 0$, $\mu_2 = 0$, $\mu_3 = 0$, $\mu_4 \neq 0$.

For the first case, the optimal solution is

$$t_1^* = 1, t_2^* = 1. \tag{98}$$

For the second case, following (95) and (96), we get

$$\cos\theta_{\text{des}} - \iota\left(t_1 \sin\theta_t \cos\theta_{\text{des}} + t_2 \sin\theta_{\text{des}} \cos\theta_t\right) = 0, \tag{99}$$

and $t_1 - 1 = 0$,which implies

$$t_1^* = 1, \;\; t_2^* = \frac{\cos\theta_{\text{des}} - \iota \sin\theta_t \cos\theta_{\text{des}}}{\iota \sin\theta_{\text{des}} \cos\theta_t}. \tag{100}$$

Similarly, for the third case, we obtain

$$t_1^* = \frac{\cos\theta_{\text{des}} - \iota \sin\theta_{\text{des}} \cos\theta_t}{\iota \sin\theta_t \cos\theta_{\text{des}}}, \;\; t_2^* = 1. \tag{101}$$

For the fourth and fifth cases, the optimal solutions are similarly obtained as:

$$t_1^* = 1, \;\; t_2^* = \frac{\cos\theta_t - \iota \sin\theta_t \cos\theta_{\text{des}}}{\iota \sin\theta_{\text{des}} \cos\theta_t}, \tag{102}$$

and

$$t_1^* = \frac{\cos\theta_t - \iota \sin\theta_{\text{des}} \cos\theta_t}{\iota \sin\theta_t \cos\theta_{\text{des}}}, \;\; t_2^* = 1. \tag{103}$$

Therefore, the optimal solution to problem (91) is given by (98), (100), (101), (102), and (103). Taking the equality constraint (37) into consideration, only the first case is valid. Accordingly, the optimal solution to problem (34) is $t_1^* = 1$, $t_2^* = 1$.

B. *Proof of Theorem 1*

1) For $0 \leq \alpha < 2$: We introduce $\Upsilon = \theta_t + \theta_{\text{des}}$ and $\Upsilon \in [0, \pi]$. Then, the problem in (39) is transformed to

$$\max_{\theta_t, \Upsilon} \; \frac{\Gamma \cos^{\alpha-2}\theta_t \cos^{\alpha-2}\left(\Upsilon - \theta_t\right) \sin^4 \Upsilon}{d_0^4}, \tag{104}$$
$$\text{s.t.} \;\; \cos\left(\Upsilon - \theta_t\right) - \iota \sin\Upsilon \geq 0, \tag{105}$$
$$\cos\theta_t - \iota \sin\Upsilon \geq 0, \tag{106}$$
$$0 \leq \theta_t \leq \frac{\pi}{2}, \tag{107}$$
$$0 \leq \Upsilon \leq \pi. \tag{108}$$

Here we first optimize θ_t by fixing Υ, the corresponding optimization problem is

$$\max_{\theta_t} \; \frac{\Gamma \cos^{\alpha-2}\theta_t \cos^{\alpha-2}\left(\Upsilon - \theta_t\right) \sin^4 \Upsilon}{d_0^4}, \tag{109}$$
$$\text{s.t.} \;\; \cos\left(\Upsilon - \theta_t\right) - \iota \sin\Upsilon \geq 0, \tag{110}$$
$$\cos\theta_t - \iota \sin\Upsilon \geq 0, \tag{111}$$
$$0 \leq \theta_t \leq \frac{\pi}{2}. \tag{112}$$

From (110) and (111),

$$\theta_t \geq \Upsilon - \arccos\left(\iota \sin\Upsilon\right), \tag{113}$$

and

$$\theta_t \leq \arccos\left(\iota \sin\Upsilon\right). \tag{114}$$

In order to guarantee the feasibility of problem (109), we have

$$\Upsilon - \arccos\left(\iota \sin\Upsilon\right) \leq \arccos\left(\iota \sin\Upsilon\right), \tag{115}$$

implying $\sin\frac{\Upsilon}{2} \leq \frac{1}{2\iota}$. Denote the objective function of problem (109) as

$$z\left(\theta_t\right) = \frac{\Gamma\cos^{\alpha-2}\theta_t\cos^{\alpha-2}\left(\Upsilon-\theta_t\right)\sin^4\Upsilon}{d_0^4}. \tag{116}$$

The derivative of function $z\left(\theta_t\right)$ is

$$\frac{\mathrm{d}z}{\mathrm{d}\theta_t} = \frac{\Gamma\left(\alpha-2\right)\sin^4\Upsilon\cos^{\alpha-3}\left(\Upsilon-\theta_t\right)\cos^{\alpha-3}\theta_t}{d_0^4}\sin\left(\Upsilon-2\theta_t\right). \tag{117}$$

Hence, given $0 \leq \alpha < 2$, $z\left(\theta_t\right)$ is monotonically decreasing for $\theta_t \leq \frac{\Upsilon}{2}$ and monotonically increasing for $\theta_t \geq \frac{\Upsilon}{2}$. Considering (113) and (114), we then obtain the maximizer $\theta_t^* = \arccos\left(\iota\sin\Upsilon\right)$ or $\theta_t^* = \Upsilon - \arccos\left(\iota\sin\Upsilon\right)$.

We then optimize Υ by setting $\theta_t^* = \arccos\left(\iota\sin\Upsilon\right)$ or $\theta_t^* = \Upsilon - \arccos\left(\iota\sin\Upsilon\right)$. The corresponding optimization problem for Υ is

$$\max_{\Upsilon} \frac{\Gamma\iota^{\alpha-2}\cos^{\alpha-2}\left(\Upsilon-\arccos\left(\iota\sin\Upsilon\right)\right)\sin^{\alpha+2}\Upsilon}{d_0^4}, \tag{118}$$

$$\text{s.t. } \sin\frac{\Upsilon}{2} \leq \frac{1}{2\iota}, \tag{119}$$

$$0 \leq \Upsilon \leq \pi. \tag{120}$$

Let $\nu = \Upsilon - \arccos\left(\iota\sin\Upsilon\right)$, thus $\sin\Upsilon = \frac{\cos\nu}{\sqrt{1+\iota^2-2\iota\sin\nu}}$. As it is seen $\nu = \Upsilon - \arccos\left(\iota\sin\Upsilon\right)$ is monotonically increasing with Υ. Therefore, from the constraint (119), we obtain $\sin\nu \leq \frac{1}{2\iota}$. Therefore, problem (118) is reduced to

$$\max_{\nu} h\left(\nu\right) = \frac{\Gamma\iota^{\alpha-2}}{d_0^4}\cos^{\alpha-2}\nu\left(\frac{\cos\nu}{\sqrt{1+\iota^2-2\iota\sin\nu}}\right)^{\alpha+2}, \tag{121}$$

$$\text{s.t. } \sin\nu \leq \frac{1}{2\iota}, \tag{122}$$

$$0 \leq \nu \leq \frac{\pi}{2}. \tag{123}$$

The maximizer of function $h\left(\nu\right)$ is given by (50). Hence, the optimal solution to problem (121) is given in (49). Using $\nu = \Upsilon - \arccos\left(\iota\sin\Upsilon\right)$, the optimal solution to problem (118) is obtained as in (48).

2) For $\alpha = 2$: We set $\Upsilon = \theta_t + \theta_{\text{des}}$ and problem (39) is rewritten as

$$\max_{\theta_t,\Upsilon} \frac{\Gamma\sin^4\Upsilon}{d_0^4}, \tag{124}$$

$$\text{s.t. } d_0\cos\left(\Upsilon-\theta_t\right) - \frac{2D^2}{\lambda}\sin\Upsilon \geq 0, \tag{125}$$

$$d_0\cos\theta_t - \frac{2D^2}{\lambda}\sin\Upsilon \geq 0, \tag{126}$$

$$0 \leq \theta_t \leq \frac{\pi}{2}, \tag{127}$$

$$0 \leq \Upsilon \leq \pi. \tag{128}$$

Similarly, we first optimize θ_t with a given Υ. The corresponding optimization problem is

$$\max_{\theta_t} \frac{\Gamma\sin^4\Upsilon}{d_0^4}, \tag{129}$$

$$\text{s.t. } \Upsilon - \arccos\left(\iota\sin\Upsilon\right) \leq \theta_t \leq \arccos\left(\iota\sin\Upsilon\right), \tag{130}$$

$$0 \leq \theta_t \leq \frac{\pi}{2}. \tag{131}$$

The optimal solution to problem (129) is

$$\theta_t^* = \left\{\theta_t^* \mid \Delta_1 \leq \theta_t^* \leq \Delta_2\right\}, \tag{132}$$

where

$$\Delta_1 = \max\left\{\Upsilon - \arccos\left(\iota\sin\Upsilon\right), 0\right\},$$

$$\Delta_2 = \min\left\{\arccos\left(\iota\sin\Upsilon\right), \frac{\pi}{2}\right\},$$

and

$$\arccos\left(\iota\sin\Upsilon\right) \geq \frac{\Upsilon}{2}. \tag{133}$$

We then further optimize Υ through the following optimization problem

$$\max_{\Upsilon} \frac{\Gamma\sin^4\Upsilon}{d_0^4}, \tag{134}$$

$$\text{s.t. } \sin\frac{\Upsilon}{2} \leq \frac{1}{2\iota}, \tag{135}$$

$$0 \leq \Upsilon \leq \pi,$$

where constraint (134) is equivalent to (133). Given $\frac{1}{2\iota} \leq 1$, the optimal solution to problem (134) is

$$\Upsilon^* = 2\arcsin\frac{1}{2\iota}. \tag{136}$$

For $\frac{1}{2\iota} > 1$, the optimal solution is

$$\Upsilon^* = \frac{\pi}{2}. \tag{137}$$

Combining (132), (136), and (137), the optimal solution to problem (39) is obtained as presented in (45).

3) For $\alpha > 2$: From (117), $z\left(\theta_t\right)$ is monotonically increasing for $\theta_t \leq \frac{\Upsilon}{2}$ and monotonically decreasing for $\theta_t \geq \frac{\Upsilon}{2}$, which implies the maximizer is $\theta_t = \frac{\Upsilon}{2}$. The maximizer obviously satisfies constraint (112). Thus, the maximizer, i.e.,

$$\theta_t^* = \frac{\Upsilon}{2}, \tag{138}$$

is the optimal solution to problem (109).

Then, for $\alpha > 2$, by using the optimal $\theta_t^* = \frac{\Upsilon}{2}$, the Υ optimization problem is give by

$$\max_{\Upsilon} \frac{\Gamma\cos^{2\alpha-4}\frac{\Upsilon}{2}\sin^4\Upsilon}{d_0^4}, \tag{139}$$

$$\text{s.t. } \cos\frac{\Upsilon}{2} - \iota\sin\Upsilon \geq 0, \tag{140}$$

$$0 \leq \Upsilon \leq \pi. \tag{141}$$

Let $u = \cos^2\frac{\Upsilon}{2}$ and problem (139) is equivalently written as

$$\max_{u} \frac{16\Gamma u^{\alpha}\left(1-u\right)^2}{d_0^4}, \tag{142}$$

$$\text{s.t. } u \geq 1 - \frac{1}{4\iota^2}, \tag{143}$$

$$0 \leq u \leq 1. \tag{144}$$

Denote

$$w\left(u\right) = \frac{16\Gamma u^{\alpha}\left(1-u\right)^2}{d_0^4}, \tag{145}$$

and we obtain

$$\frac{\mathrm{d}w}{\mathrm{d}u} = \frac{16\Gamma u^{\alpha-1}\left(1-u\right)}{d_0^4}\left(\alpha - \left(\alpha+2\right)u\right), \tag{146}$$

which implies the maximizer of function w is $u = \frac{\alpha}{\alpha+2}$. However, considering the constraint (143), we characterize the optimal solution to problem (142) as

$$u^* = \begin{cases} \frac{\alpha}{\alpha+2}, & \frac{1}{4\iota^2} \geq \frac{2}{\alpha+2}, \\ 1 - \frac{1}{4\iota^2}, & \frac{1}{4\iota^2} < \frac{2}{\alpha+2}. \end{cases} \tag{147}$$

Finally, by using (138), (147), and $u = \cos^2 \frac{\Upsilon}{2}$, the optimal solution to problem (39) is given by Theorem 1. This completes the proof.

C. Proof of Proposition 2

Given θ_t and θ_{des} for the problem in (53), the optimal φ_t^* and φ_{des}^* are obtained by using constraints (56) and (57), i.e.,

$$\tan\theta_t \left|\cos\varphi_t\right| = \tan\theta_{\text{des}} \left|\cos\varphi_{\text{des}}\right|, \tag{148}$$

$$\tan\theta_t \left|\sin\varphi_t\right| + \tan\theta_{\text{des}} \left|\sin\varphi_{\text{des}}\right| = \frac{d_0}{H}. \tag{149}$$

Furthermore, we note that $\sin^2\varphi_t + \cos^2\varphi_t = 1$ and $\sin^2\varphi_{\text{des}} + \cos^2\varphi_{\text{des}} = 1$, thus the solutions of φ_t^* and φ_{des}^* must satisfy

$$\left|\sin\varphi_t^*\right| = \frac{\tan^2\theta_t - \tan^2\theta_{\text{des}} + \frac{d_0^2}{H^2}}{2\frac{d_0}{H}\tan\theta_t}, \tag{150}$$

$$\left|\sin\varphi_{\text{des}}^*\right| = \frac{\tan^2\theta_{\text{des}} - \tan^2\theta_t + \frac{d_0^2}{H^2}}{2\frac{d_0}{H}\tan\theta_{\text{des}}}. \tag{151}$$

Therefore, from (150) and (151), (61) and (62) are obtained. This completes the proof.

D. Proof of Theorem 2

In order to solve problem (65), we first optimize θ_t with a given θ_{des}. The corresponding optimization problem is

$$\begin{aligned} \max_{\theta_t} \ & \frac{\Gamma\cos^{\alpha+2}\theta_t \cos^{\alpha+2}\theta_{\text{des}}}{H^4}, \\ \text{s.t.} \ & \cos\theta_t \leq \frac{H\lambda}{2D^2}, \\ & 0 \leq \cos\theta_t \leq 1. \end{aligned} \tag{152}$$

Given the monotonicity of the objective function with respect to θ_t, the optimal solution to problem (152) is

$$\theta_t^* = \arccos\Delta. \tag{153}$$

Taking the optimal solution (153) into problem (65), we then optimize θ_{des} through the following optimization problem

$$\begin{aligned} \max_{\theta_{\text{des}}} \ & \frac{\Gamma\cos^{\alpha+2}\theta_t^* \cos^{\alpha+2}\theta_{\text{des}}}{H^4}, \\ \text{s.t.} \ & \cos\theta_{\text{des}} \leq \frac{H\lambda}{2D^2}, \\ & 0 \leq \cos\theta_{\text{des}} \leq 1. \end{aligned} \tag{154}$$

The optimal solution to problem (154) is then obtained as

$$\theta_{\text{des}}^* = \theta_t^* = \arccos\Delta, \tag{155}$$

which completes the proof.

E. Proof of Theorem 3

Let $t = |\sin\varphi|$. In the following, we first optimize t for a given θ through the following optimization problem

$$\max_t \ 16\Gamma t^4 \cos^{2\alpha}\theta \sin^4\theta, \tag{156}$$

$$\text{s.t. } t \leq \frac{1}{2\iota\sin\theta}, \tag{157}$$

$$0 \leq t \leq 1. \tag{158}$$

Denote

$$q(t) = 16\Gamma t^4 \cos^{2\alpha}\theta \sin^4\theta,$$

which is a monotonically increasing function of t. Hence, the optimal solution to problem (156) is given for the following

$$t^* = \begin{cases} \frac{1}{2\iota\sin\theta}, & \frac{1}{2\iota\sin\theta} \leq 1, \\ 1, & \frac{1}{2\iota\sin\theta} \geq 1. \end{cases}$$

In the following, using t^*, we further optimize the elevation angles, θ. The corresponding optimization problem for case 1 and 2 are:

$$\text{case 1: } \max_\theta \ 16\Gamma\cos^{2\alpha}\theta\sin^4\theta, \tag{159}$$

$$\text{s.t. } \frac{1}{2\iota\sin\theta} \geq 1, \tag{160}$$

$$0 \leq \theta \leq \frac{\pi}{2}. \tag{161}$$

and

$$\text{case 2: } \max_\theta \ \frac{\Gamma}{\iota^4}\cos^{2\alpha}\theta, \tag{162}$$

$$\text{s.t. } \frac{1}{2\iota\sin\theta} \leq 1, \tag{163}$$

$$0 \leq \theta \leq \frac{\pi}{2}. \tag{164}$$

Introducing $u = \cos^2\theta$, problem (159) is transformed into problem (142) in the proof of Theorem 1, and thus the optimal solution is

$$u^* = \begin{cases} \frac{\alpha}{\alpha+2}, & \frac{1}{4\iota^2} \geq \frac{2}{\alpha+2}, \\ 1 - \frac{1}{4\iota^2}, & \frac{1}{4\iota^2} < \frac{2}{\alpha+2}. \end{cases} \tag{165}$$

Setting $u = \cos^2\theta$, problem (162) is reduced to

$$\max_\theta \ q_2 = \frac{\Gamma}{\iota^4}u^\alpha, \tag{166}$$

$$\text{s.t.} u \leq 1 - \frac{1}{4\iota^2}, \tag{167}$$

$$0 \leq u \leq 1. \tag{168}$$

Suppose that $\frac{1}{4\iota^2} \leq 1$, the optimal solution to problem (166) is then obtained as

$$u^* = 1 - \frac{1}{4\iota^2}. \tag{169}$$

The problem in (166) is however infeasible for $\frac{1}{4\iota^2} > 1$, this results in the second case to be infeasible.

In order to achieve the optimal solution to problem (159), we should take the maximum objective value of problem (159)

and problem (162). For the first case, by using (165), the optimal solution to problem (142) is

$$\theta^* = \begin{cases} \arccos\left(\sqrt{\frac{\alpha}{\alpha+2}}\right), & \frac{1}{4\iota^2} \geq \frac{2}{\alpha+2}, \\ \arccos\left(\sqrt{1-\frac{1}{4\iota^2}}\right), & \frac{1}{4\iota^2} \leq \frac{2}{\alpha+2}, \end{cases} \tag{170}$$

and hence the optimal objective value is

$$q_1 = \begin{cases} 16\Gamma\left(\frac{\alpha}{\alpha+2}\right)^3\left(\frac{2}{\alpha+2}\right)^2, & \frac{1}{4\iota^2} \leq \frac{2}{\alpha+2}, \\ 16\Gamma\left(1-\frac{1}{4\iota^2}\right)^3\left(\frac{1}{4\iota^2}\right)^2, & \frac{1}{4\iota^2} > \frac{2}{\alpha+2}. \end{cases} \tag{171}$$

In addition, by using (169), the optimal solution to problem (166) is

$$\theta^* = \arccos\left(\sqrt{1-\frac{1}{4\iota^2}}\right), \frac{1}{4\iota^2} \leq 1,$$

and the corresponding optimal objective value is

$$q_2 = 16\Gamma\left(1-\frac{1}{4\iota^2}\right)^3\left(\frac{1}{4\iota^2}\right)^2, \ \frac{1}{4\iota^2} \leq 1. \tag{172}$$

Note that

$$\max\{q_1, q_2\} = q_1,$$

implying the adoption of the first case. Therefore, the optimal solution to problem (156) is (170) and $t^* = 1$, which results in (77). This completes the proof.

F. Proof of Theorem 4

Here we first assume θ is given and find the optimized value of φ. The corresponding problem is

$$\max_{\varphi} \ v_2(\theta, \varphi) = \frac{\Gamma \cos^{4+2\alpha}\theta}{H^4}, \tag{173}$$

$$\text{s.t.} \ \frac{2H}{\cos\theta}\sin\theta\,|\sin\varphi| = d_0, \tag{174}$$

$$0 \leq \varphi \leq 2\pi.$$

The optimal solution to problem (173) is then obtained by applying the constraint (173), which is given in (87).

We then optimize θ via the following optimization problem:

$$\max_{\theta} \ \frac{\Gamma \cos^{4+2\alpha}\theta}{H^4}, \tag{175}$$

$$\text{s.t.} \ \frac{H}{\cos\theta} \geq \frac{2D^2}{\lambda},$$

$$0 \leq \theta \leq \frac{\pi}{2}.$$

Noting that the objective function is a monotonically decreasing function of θ, the optimal solution is obtained as in (86).

REFERENCES

[1] W. Saad, M. Bennis, and M. Chen, "A vision of 6G wireless systems: Applications, trends, technologies, and open research problems," *IEEE Netw.*, vol. 34, pp. 134–142, Oct. 2020.

[2] K. David and H. Berndt, "6G vision and requirements: Is there any need for beyond 5G?," *IEEE Veh. Tech. Mag.*, vol. 13, pp. 72–80, Jul. 2018.

[3] A. Al-Fuqaha, M. Guizani, M. Mohammadi, M. Aledhari, and M. Ayyash, "Internet of things: A survey on enabling technologies, protocols, and applications," *IEEE Commun. Surveys Tuts.*, vol. 17, pp. 2347–2376, Jun. 2015.

[4] V. Jungnickel, K. Manolakis, W. Zirwas, B. Panzner, V. Braun, M. Lossow, M. Sternad, R. Apelfrojd, and T. Svensson, "The role of small cells, coordinated multipoint, and massive MIMO in 5G," *IEEE Commun. Mag.*, vol. 52, pp. 44–51, May 2014.

[5] M. Xiao, S. Mumtaz, Y. Huang, L. Dai, Y. Li, M. Matthaiou, G. K. Karagiannidis, E. Bjornson, K. Yang, C. I, and A. Ghosh, "Millimeter wave communications for future mobile networks," *IEEE J. Sel. Areas Commun.*, vol. 35, pp. 1909–1935, Jun. 2017.

[6] J. Wang, W. Guan, Y. Huang, R. Schober, and X. You, "Distributed optimization of hierarchical small cell networks: A GNEP framework," *IEEE J. Sel. Areas Commun.*, vol. 35, pp. 249–264, Feb. 2017.

[7] W. Tang, M. Z. Chen, J. Y. Dai, Y. Zeng, X. Zhao, S. Jin, Q. Cheng, and T. J. Cui, "Wireless communications with programmable metasurface: New paradigms, opportunities, and challenges on transceiver design," *IEEE Wireless Commun.*, vol. 27, pp. 180–187, Mar. 2020.

[8] J. Zhao and Y. Liu, "A survey of intelligent reflecting surfaces (IRSs): Towards 6G wireless communication networks," *arXiv preprint arXiv:1907.04789*, 2019.

[9] W. Tang, M. Z. Chen, X. Chen, J. Y. Dai, Y. Han, M. Di Renzo, Y. Zeng, S. Jin, Q. Cheng, and T. J. Cui, "Wireless communications with reconfigurable intelligent surface: Path loss modeling and experimental measurement," *IEEE Trans. on Wireless Commun.*, vol. 20, pp. 421–439, Sep. 2021.

[10] Q. Wu and R. Zhang, "Beamforming optimization for wireless network aided by intelligent reflecting surface with discrete phase shifts," *IEEE Trans. on Commun.*, vol. 68, pp. 1838–1851, Dec. 2020.

[11] J. Chen, Y.-C. Liang, Y. Pei, and H. Guo, "Intelligent reflecting surface: A programmable wireless environment for physical layer security," *IEEE Access*, vol. 7, pp. 82599–82612, Jun. 2019.

[12] M. Di Renzo, M. Debbah, D.-T. Phan-Huy, A. Zappone, M.-S. Alouini, C. Yuen, V. Sciancalepore, G. C. Alexandropoulos, J. Hoydis, H. Gacanin, *et al.*, "Smart radio environments empowered by AI reconfigurable meta-surfaces: An idea whose time has come," *EURASIP J. Wireless Commun. Netw.*, pp. 1–20, May 2019.

[13] Q. Wu and R. Zhang, "Intelligent reflecting surface enhanced wireless network via joint active and passive beamforming," *IEEE Trans. on Wireless Commun.*, vol. 18, pp. 5394–5409, Aug. 2019.

[14] M. Fu, Y. Zhou, and Y. Shi, "Intelligent reflecting surface for downlink non-orthogonal multiple access networks," in *Proc. IEEE Globecom Workshops*, (Waikoloa, HI), pp. 1–6, Dec. 2019.

[15] J. He, H. Wymeersch, L. Kong, O. Silven, and M. Juntti, "Large intelligent surface for positioning in millimeter wave MIMO systems," in *Proc. IEEE 91st VTC-Spring*, (Antwerp, Belgium), pp. 1–5, May 2020.

[16] S. Hu, F. Rusek, and O. Edfors, "Beyond massive MIMO: The potential of positioning with large intelligent surfaces," *IEEE Trans. on Signal Process.*, vol. 66, pp. 1761–1774, Jan. 2018.

[17] Z. Ding and H. V. Poor, "A simple design of IRS-NOMA transmission," *IEEE Commun. Lett.*, vol. 24, pp. 1119–1123, Feb. 2020.

[18] J. Zhu, Y. Huang, J. Wang, K. Navaie, and Z. Ding, "Power efficient IRS-assisted NOMA," *IEEE Trans. on Commun.*, vol. 69, pp. 900–913, Oct. 2021.

[19] X. Mu, Y. Liu, L. Guo, J. Lin, and N. Al-Dhahir, "Exploiting intelligent reflecting surfaces in multi-antenna aided NOMA systems," *arXiv preprint arXiv:1910.13636*, 2019.

[20] X. Guan, Q. Wu, and R. Zhang, "Intelligent reflecting surface assisted secrecy communication: Is artificial noise helpful or not?," *IEEE Wireless Commun. Lett.*, vol. 9, pp. 778–782, Jan. 2020.

[21] X. Yu, D. Xu, and R. Schober, "Enabling secure wireless communications via intelligent reflecting surfaces," in *Proc. IEEE GLOBECOM*, (Waikoloa, HI, USA), pp. 1–6, Feb. 2019.

[22] H. Shen, W. Xu, S. Gong, Z. He, and C. Zhao, "Secrecy rate maximization for intelligent reflecting surface assisted multi-antenna communications," *IEEE Commun. Lett.*, vol. 23, pp. 1488–1492, Jun. 2019.

[23] P. Wang, J. Fang, X. Yuan, Z. Chen, and H. Li, "Intelligent reflecting surface-assisted millimeter wave communications: Joint active and passive precoding design," *IEEE Trans. on Veh. Technol.*, vol. 69, pp. 14960–14973, Oct. 2020.

[24] Y. Zhu, G. Zheng, and K.-K. Wong, "Stochastic geometry analysis of large intelligent surface-assisted millimeter wave networks," *IEEE J. Sel. Areas Commun.*, vol. 38, pp. 1749–1762, Jun. 2020.

[25] Q. Wu and R. Zhang, "Joint active and passive beamforming optimization for intelligent reflecting surface assisted SWIPT under QoS constraints," *IEEE J. Sel. Areas Commun.*, vol. 38, pp. 1735–1748, Jul. 2020.

[26] Q. Wu and R. Zhang, "Weighted sum power maximization for intelligent reflecting surface aided SWIPT," *IEEE Wireless Commun. Lett.*, vol. 9, pp. 586–590, Dec. 2020.

[27] K. Feng, Q. Wang, X. Li, and C. Wen, "Deep reinforcement learning based intelligent reflecting surface optimization for MISO communication systems," *IEEE Wireless Commun. Lett.*, vol. 9, pp. 745–749, Jan. 2020.

[28] H. Yang, Z. Xiong, J. Zhao, D. Niyato, Q. Wu, H. V. Poor, and M. Tornatore, "Intelligent reflecting surface assisted anti-jamming communications: A fast reinforcement learning approach," *IEEE Trans. on Wireless Commun.*, vol. 20, pp. 1963–1974, Nov. 2021.

[29] S. Li, B. Duo, X. Yuan, Y. Liang, and M. Di Renzo, "Reconfigurable intelligent surface assisted UAV communication: Joint trajectory design and passive beamforming," *IEEE Wireless Commun. Lett.*, vol. 9, pp. 716–720, Jan. 2020.

[30] D. Ma, M. Ding, and M. Hassan, "Enhancing cellular communications for UAVs via intelligent reflective surface," in *Proc. IEEE WCNC*, (Seoul, Korea (South)), pp. 1–6, Jun. 2020.

[31] Q. Wu and R. Zhang, "Towards smart and reconfigurable environment: Intelligent reflecting surface aided wireless network," *IEEE Commun. Magazine*, vol. 58, pp. 106–112, Nov. 2020.

[32] H. Lu, Y. Zeng, S. Jin, and R. Zhang, "Aerial intelligent reflecting surface: Joint placement and passive beamforming design with 3D beam flattening," *IEEE Trans. on Wireless Commun.*, pp. 1–1, Feb. 2021.

[33] G. Zhou, C. Pan, H. Ren, K. Wang, and A. Nallanathan, "A framework of robust transmission design for IRS-aided MISO communications with imperfect cascaded channels," *IEEE Trans. on Signal Process.*, vol. 68, pp. 5092–5106, 2020.

[34] Q. Wu and R. Zhang, "Weighted sum power maximization for intelligent reflecting surface aided SWIPT," *IEEE Wireless Commun. Lett.*, vol. 9, pp. 586–590, Dec. 2020.

[35] W. L. Stutzman and G. A. Thiele, *Antenna theory and design*. John Wiley & Sons, 2012.

[36] S. Boyd and L. Vandenberghe, *Convex optimization*. Cambridge university press, 2004.